frontiers in Molecular Biosciences

ORIGINAL RESEARCH
published: 15 April 2021
doi: 10.3389/fmolb.2021.609654

Light-Driven CO_2 Reduction by Co-Cytochrome b_{562}

*Rafael Alcala-Torano, Nicholas Halloran, Noah Gwerder, Dayn J. Sommer and Giovanna Ghirlanda**

School of Molecular Sciences, Arizona State University, Tempe, AZ, United States

The current trend in atmospheric carbon dioxide concentrations is causing increasing concerns for its environmental impacts, and spurring the developments of sustainable methods to reduce CO_2 to usable molecules. We report the light-driven CO_2 reduction in water in mild conditions by artificial protein catalysts based on cytochrome b_{562} and incorporating cobalt protoporphyrin IX as cofactor. Incorporation into the protein scaffolds enhances the intrinsic reactivity of the cobalt porphyrin toward proton reduction and CO generation. Mutations around the binding site modulate the activity of the enzyme, pointing to the possibility of further improving catalytic activity through rational design or directed evolution.

Keywords: cobalt porphyrin, Carbon fixation, CO_2 reduction, catalysis, protein design, proton reduction

OPEN ACCESS

Edited by:
Nikolaos E. Labrou, Agricultural University of Athens, Greece

Reviewed by:
Kamlendra Singh, Karolinska Institute, Sweden
Christopher Berndsen, James Madison University, United States

****Correspondence:***
Giovanna Ghirlanda
gghirlanda@asu.edu

Specialty section:
This article was submitted to Protein Chemistry and Enzymology, a section of the journal Frontiers in Molecular Biosciences

Received: *23 September 2020*
Accepted: *11 January 2021*
Published: *15 April 2021*

Citation:
Alcala-Torano R, Halloran N, Gwerder N, Sommer DJ and Ghirlanda G (2021) Light-Driven CO_2 Reduction by Co-Cytochrome b_{562}. Front. Mol. Biosci. 8:609654. doi: 10.3389/fmolb.2021.609654

INTRODUCTION

The ongoing use of fossil fuels has led to an increase in atmospheric CO_2 concentrations, causing severe consequences for the environment (Lacis et al., 2010). Current research efforts are focused on developing energetic alternatives that can help curb CO_2 emissions. Although nature aids in the removal of this greenhouse gas through photosynthesis (Sun et al., 2014; Kondo et al., 2018), negative emissions technologies are necessary to reduce the excess gas from the atmosphere (Smith et al., 2015). One possible path is through artificial photosynthesis, where light is utilized as the energy source to drive production of carbon-free or carbon-neutral fuels, mirroring the role of the enzyme RuBisCO in fixing CO_2. In that vein, promising approaches interfacing photosensitizers and/or materials with molecular catalysts, enzymes, and microorganisms have been developed (Woo, 2017; Luan and Lu, 2018; Edwards and Bren, 2020; Ma et al., 2020).

Artificial metalloenzymes obtained by incorporating organometallic catalysts within a protein bridge traditional molecular catalysts and enzymes, with the advantage of expanding the range of reactivity encountered in natural enzymes. Protein scaffolds may aide the efficiency of the organometallic center by offering tunable primary and secondary coordination spheres, by facilitating reactant binding and product release to and from the active site, and by protecting the organometallic center from degradation (Lu et al., 2009; Alcala-Torano et al., 2016; Schwizer et al., 2018; Davis and Ward, 2019; Nastri et al., 2019; Oohora et al., 2019; Vornholt et al., 2020). This approach has been used to produce water-soluble catalysts that are capable of producing hydrogen from protons under mild conditions, repurposing a diverse group of organometallic catalysts (Sano et al., 2011; Roy et al., 2012; Kleingardner et al., 2014; Onoda et al., 2014; Sommer et al., 2014; Sommer et al., 2016; Firpo et al., 2018; Call et al., 2019a; Slater et al., 2019; Walsh et al., 2019; Alvarez-Hernandez et al., 2020; Laureanti et al., 2020; Le et al., 2020; Roy et al., 2020). Comparatively little work has been carried out on the reduction of CO_2 by hybrid metalloenzymes: in one example nickel cyclam complexes anchored to azurin support catalytic CO_2 reduction, with evidence of protein

modulation of activity compared to the isolated cyclam (Schneider and Shafaat, 2016; Liu et al., 2018; Schneider et al., 2018).

Here, we investigate whether coordination of CoPPIX within a protein scaffold would support carbon dioxide reduction, motivated by recent reports of metalloporphyrins as molecular CO_2 reduction electrocatalysts (Manbeck and Fujita, 2015; Mondal et al., 2015; Zhang et al., 2017; Birdja et al., 2018; Rao et al., 2018) and most recently photocatalysts (Call et al., 2019b; Fukuzumi et al., 2019). In these catalysts, tuning the reaction conditions or modifying the porphyrin framework in order to stabilize catalytic intermediates through hydrogen bonding resulted in increased activities of these catalysts toward CO_2 reduction (Bhugun et al., 1996; Lee et al., 2011; Costentin et al., 2012; Azcarate et al., 2016a; b; Call et al., 2019b). Further, increased turnover numbers (TON) and product selectivity upon incorporation of cobalt porphyrins into supramolecular structures such as metal-organic frameworks (Kornienko et al., 2015; Lin et al., 2015; Zhang et al., 2016; Feng et al., 2020; Wu et al., 2020; Zhang et al., 2020) and polymers (Kramer and McCrory, 2016; Liu and McCrory, 2019) suggest that catalysis by cobalt porphyrins could be enhanced by incorporation into a protein environment. Our approach utilizes a natural protein scaffold, cytochrome b_{562} (cyt b_{562}), in which the native heme has been swapped with its cobalt analog, cobalt protoporphyrin IX (CoPPIX). Our group and others have previously demonstrated that exchanging the metal ion to cobalt in heme-binding proteins or peptides results in metalloproteins that can catalyze proton reduction activity, and show an increase of H_2 production compared to the cobalt porphyrin in solution. Moreover, altering the protein sequence results in fine modulation of the total activity, further supporting the crucial role of the protein environment throughout the catalytic cycle, beyond simple encapsulation (Kleingardner et al., 2014; Sommer et al., 2014; Sommer et al., 2016; Firpo et al., 2018; Le and Bren, 2019; Alvarez-Hernandez et al., 2020; Le et al., 2020). Compared with other supramolecular systems, proteins are easily modifiable by mutating the amino acid sequence, allowing the systematic exploration of the primary and secondary coordination sphere. Recent advances dramatically expand the range of chemical moieties available on the side chains through incorporation of noncanonical amino acids (Alcala-Torano et al., 2016; Burke et al., 2019; Drienovská et al., 2020; Drienovská and Roelfes, 2020; Zhou and Roelfes, 2020). Further, proteins can be optimized by directed evolution coupled with high-thrughput screening to identify favorable mutations (Liang et al., 2019; Chen and Arnold, 2020; Jeong et al., 2020; Markel et al., 2020).

MATERIAL AND METHODS

All chemicals were purchased from Sigma-Aldrich and used without further purification unless otherwise noted. Calibration gases were obtained from Matheson in 14 L lecture bottles. All aqueous solutions were prepared using deionized water with a resistivity greater or equal to 18 MΩ. Cobalt (III) protoporphyrin IX chloride was purchased from Sigma-Aldrich and used without further purification.

Protein Expression

Mutants were generated in a pET30c (+) vector encoding WT cyt b_{562} using mutagenic primers by Gibson assembly as described in Supplementary Information (**Supplementary Table S1** and **Supplementary Figure S8**) (Sommer et al., 2016). The verified mutants were transformed into *Escherichia coli* BL21 (DE3) and grown in 1 L of 2xTY media at 37 °C with shaking at 300 rpm. Cells were induced with 1 mM IPTG at an OD_{600} of 0.6 and harvested after 4 h of expression. The cell pellets were suspended in 20 mM Tris-HCl, 1 mM DTT, 0.5 mM EDTA and lysed by multiple cycles of ultrasonication. The clarified lysate was brought to 75% saturation with solid ammonium sulfate, and precipitated proteins were removed by centrifugation. The supernatant, containing the cytochrome mutants, was dialyzed against two changes of 10 mM Tris pH 7.5 and one of water at 4 °C. Following dialysis, the protein solution was lyophilized and redissolved in 10 mM NaCl water for further purification via RP-HPLC, using a semi-preparatory scale C18 column with a linear 1% min^{-1} gradient from 100% solvent A (0.1% v/v TFA in water) to 100% solvent B (4.9% v/v water, 0.1% v/v TFA in acetonitrile). The fractions containing the desired protein were then lyophilized to yield the pure apo-protein. The protein identities were confirmed via MALDI-TOF-MS and their purity determined by C18 analytical analysis (Supplementary Information, **Supplementary Figure S9**). The purified protein was lyophilized and stored at −78 °C. Protein stocks were prepared by dissolving the protein in the appropriate phosphate buffer. The protein stock concentration was determined by UV spectroscopy in 6 M urea using an extinction coefficient of 2980 M^{-1} cm^{-1} at 280 nm.

Binding Assays

The dissociation constant (K_d) of each mutant was assessed by titrating a solution of CoPPIX in 200 mM potassium phosphate buffer at pH 7.5 with a solution of the apo protein, and monitoring the absorbance of the Soret peak corresponding to the holo protein (~425 nm depending on the mutant) (**Supplementary Figure S2**). The initial CoPPIX concentration was determined using the observed absorbance value at the Soret peak of the free porphyrin (417 nm) and ε = 143,540 M^{-1} cm^{-1} (as determined by ICP-OES experiments). All titrations were carried out in an anaerobic chamber (Coy Laboratory Products) equipped with UV-Vis (Ocean Optics USB4000). Data were fitted to **Eq. 1** using OriginLab as described in the Supplementary Information by adapting established procedures (Hulme and Trevethick, 2010; Kovacs et al., 2010; Thordarson, 2011).

$$\Delta A = \frac{\Delta\varepsilon}{2}\Big([Cyt]_T + [CoPPIX]_T + K_d - \sqrt{\left([Cyt]_T + [CoPPIX]_T + K_d\right)^2 - 4[CoPPIX]_T[Cyt]_T}\Big), \quad (1)$$

ΔA and $\Delta\varepsilon$ are the differences in absorbance and in extinction coefficients, respectively, between the free porphyrin and the holo protein at the latter's Soret peak (~425 nm). $[CoPPIX]_T$ is the

total CoPPIX concentration, and $[Cyt]_T$ is the total protein concentration after each addition.

Circular Dichroism Spectroscopy

CD spectra were recorded on a JASCO J-815 spectropolarimeter in the range of 200–280 nm using a 1 mm cuvette. Data points were recorded every 1 nm and averaged over three scans. The protein concentration was kept at 5 μM in 10 mM phosphate buffer pH 7.5 and the spectra was recorded at 20 °C. Holo protein measurements were carried out in excess CoPPIX (20 μM). Thermal denaturation was performed by heating samples from 4 to 90 °C at a rate of 1°C min^{-1}, monitoring the loss of signal at 222 nm.

Photocatalytic Experiments

Reactions were carried out in sealed cuvettes. Stock buffer containing 200 mM potassium phosphate and 125 mM ascorbic acid at pH 6.0 was bubbled with either CO_2 or Ar, and adjusted back to pH 6.0 with aqueous KOH if necessary. Finally, solid $[Ru(bpy)_3]Cl_2 \cdot 6\ H_2O$ was added to a 1.25 mM final concentration, flash frozen in aliquots, and stored at −80 °C. Before each assay, CoPPIX was dissolved in 100 mM KOH to make a saturated solution, and the stock concentration was determined by UV-Vis using the Soret peak at 417 nm with an extinction coefficient of ε = 143,540 M^{-1} cm^{-1} (as determined by ICP-OES measurements). The frozen buffer was thawed under an atmosphere of either CO_2 or Ar, and CoPPIX and/or protein (in 200 mM potassium phosphate) added to obtain working solutions containing 20 μM CoPPIX, 30 μM protein, 100 mM ascorbic acid, and 1 mM $[Ru(bpy)_3]^{2+}$ in 200 mM potassium phosphate. The ratio of CoPPIX to apo protein was chosen from equilibrium calculations based on the highest observed K_d value to ensure ≥95% of porphyrin was bound to the protein.

For each experiment, 400 μL of sample was added to a 10 mm × 1 mm gas tight cuvette of known headspace volume, and the headspace sparged with gas (Ar or CO_2) for 20 min. The cuvettes were then irradiated with a white light LED source for 8 h. All experiments were done in triplicate and the variation is reported as the standard deviation of the sample. The gaseous products, H_2 and CO, were quantified by removing 100 μL from the headspace at time intervals, and analyzed with an SRI Instruments gas chromatograph equipped with a 3 ft × 1/8" molecular sieve 5 Å packed column. H_2 and CO were detected and quantified simultaneously from the same injection using a Thermal Conductivity Detector (TCD) and a Flame ionization Detector (FID) with a methanizer connected in series. The analytes were eluted using Ar as a carrier gas with a temperature program starting at 60 °C for 1 min, ramping at 20 °C min^{-1} until 80°C, holding for 2 min, ramping at 50 °C min^{-1} to 250°C, and holding until the CO_2 exited the instrument, with a retention time (t_R) ca. 12 min. A peak corresponding to H_2 was seen on the TCD channel at t_R of 0.400 min, while the peak corresponding to CO appeared at t_R = 3.42 min on the FID channel. Peak areas were converted to moles using a calibration curve (**Supplementary Figures S4** and **S5**). After irradiation was stopped, the solution was frozen at −80 °C for future analysis. Formate was quantified by diluting the sample to 10% v/v D_2O in water and 100 μM sodium 4,4-dimethyl-1-silapentane-1- sulfonate (DSS) as an internal standard. The samples were then analyzed by ^1H NMR using a water suppression method with 64 scans and a 30 s relaxation delay. The formate concentration was determined by comparing the integration area of the singlet at 8.45 ppm to the DSS peak at 0.0 ppm (Boston et al., 2013; Yehezkeli et al., 2016).

Turnover numbers (TON) are reported as the ratio of moles of product produced by moles of total CoPPIX present in solution. Comparisons between the means of each experiment were assessed using a two-tailed *t*-test analysis for samples with equal or unequal variances as determined by Levene's test. The null hypothesis (H_0: $\bar{x}_1 - \bar{x}_2 = 0$) was rejected for *p*-values < 0.05. The calculated *p*-values can be found in **Supplementary Tables S2–S4** in the Supplementary Information.

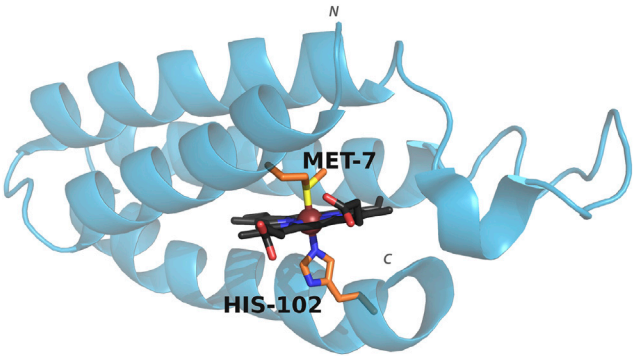

FIGURE 1 | Structure of cyt b_{562} showing the coordinating axial ligands. PDB entry: 1QPU. Colors represent carbon (porphyrin: black, axial residues: orange), oxygen (red), nitrogen (blue), sulfur (yellow). The metal ion is shown as a sphere (brown). The *N* and *C* terminus are indicated.

RESULTS AND DISCUSSION

Protein Design

Cyt b_{562} is a small, water-soluble, four-helix bundle that natively binds a heme cofactor via bis-axial ligation from the side chains of residues His102 and Met7 (**Figure 1**), and can coordinate a wide range of metalloporphyrins (Pia et al., 2012; Sommer et al., 2016; Bowen et al., 2020). Swapping in CoPPIX for heme and assessing activity under photocatalytic conditions results in a 10 fold increase in hydrogen production compared to CoPPIX in solution (Sommer et al., 2016). In order to facilitate binding of carbon dioxide and conversion to product, we utilized mutants that either remove axial ligation sites (M7A and H102A) or alter axial ligation (M7H) (Kamiya et al., 2001; Hay and Wydrzynski, 2005; Sommer et al., 2016). We assessed the effect of these mutations on the efficiency and specificity of CO_2 reduction in water by cobalt porphyrins, which yields formate, carbon monoxide, and hydrogen in photocatalytic conditions.

We investigated the secondary structure and stability of the mutant proteins in the apo state and in response to binding to CoPPIX. The CD spectra of all apo mutants showed the typical

TABLE 1 | CD and binding data for Co-cyt b_{562} mutants. CD spectra was obtained at 20 °C in 10 mM phosphate buffer pH 7.5 with a protein concentration of 5 μM and CoPPIX concentration of 20 μM. The K_d values were obtained using UV-Vis spectroscopy by titrating a stock solution of apo protein to a solution of CoPPIX of known concentration (see Methods and **Supplementary Figures S1 and S2**).

Mutant	T_m (°C)		ΔT_m (°C)	K_d (nM)
	Apo	Holo		
WT	56	72	+16	45 ± 19
M7A	52	65	+13	175 ± 22
M7H	50	75	+25	559 ± 89
H102A	57	56	−1	81 ± 54

signals of α-helical proteins, with local minima at 208 and 222 nm (Supplementary Information, **Supplementary Figure S1**). Upon reconstitution with CoPPIX, WT and M7A show minimal changes in this region, indicating that incorporation of the cofactor has little effect on the structure of the protein at room temperature. The signal for M7H increases upon addition of the porphyrin, showing that incorporation of the ligand stabilizes the secondary structure of the protein, possibly because coordination to the metal reduces the buried positive charges related to the two abutting histidines in the unoccupied active site. In contrast, H102A shows a decrease in signal upon addition of the porphyrin suggesting that this mutant adopts different apo and bound structures compared to the other mutants in the series (see discussion below).

More information on structural changes upon binding was gathered by comparing the stability of the mutants in the apo and holo state. We carried out unfolding experiments by monitoring the loss of intensity of the 222 nm peak in the CD spectrum at increasing temperature, obtaining thermal denaturation curves of the apo and holo mutants (SI, **Supplementary Figure S1**). The data presented in **Table 1** shows that the apparent midpoint of the thermal denaturation, T_m, increases significantly upon binding of the porphyrin, with the exception of H102A, which showed a minimal change in its T_m value.

The stability of the apo state is strongly affected by mutations: compared to WT, the T_m of M7A is lowered 4 °C, possibly due to a decrease in core hydrophobic volume, balanced by the high helical propensity of alanine compared to methionine (Chakrabartty et al., 1991). M7H experiences a 6 °C destabilization. The solution structure of WT apo cyt b_{562} (Feng et al., 1994) shows that His7 is largely solvent accessible, suggesting a pK_a close to neutrality and indicating that the side chain can be partially charged under the experimental conditions (Edgcomb and Murphy, 2002). The observed destabilization correlates to lower helical propensity of histidine—particularly when ionized—compared to methionine (Pace and Scholtz, 1998). In contrast, H102A displays stability slightly higher than WT, because of the high helical propensity of alanine. Binding to CoPPIX stabilizes the proteins to an extent that reflects the changes in axial ligation: M7A is stabilized by 13 °C, a lesser extent than observed in WT (16 °C) because of the loss of axial ligand, while M7H experiences much higher stabilization (25 °C) because of the strong double axial ligation afforded by histidine, and the loss of buried charges upon coordination. In H102A, however, binding to CoPPIX does not increase stability. We speculate that comparable helical content and stabilities between the apo forms of H102A and WT arise from the small contribution of the C-terminal α-helix to the folding of apo cyt b_{562}, because the C-terminus is unfolded in solution (PDB 1APC) (Feng et al., 1994). This observation suggests that folding of the C-terminal α-helix in the holo state of WT is predominantly driven by ligation of His102 to the porphyrin, and abolishing this interaction in H102A prevents folding of the bundle. In contrast, mutations to the axial position M7 have minimal effect on the stability of the holo protein: M7A is slightly destabilized compared to WT, while M7H displays higher apparent T_m, reflecting the relative strength of the axial coordination.

All mutants bind CoPPIX with K_d values in the low to mid-nanomolar range, as assessed through UV-Vis titration of apo protein to a solution of CoPPIX (SI, **Supplementary Figure S2** and **Table 1**). However, displacement of either one of the native axial ligands weakens affinity, and all mutants bind CoPPIX with higher K_d values than WT. Among the mutants, H102A displays the highest affinity, similar to WT, followed by M7A; M7H registers the weakest affinity by far. This observation suggests that binding of the cofactor requires a pre-structured binding pocket in the apo state, as the affinity trend mirrors the trend observed for the stability of the apo forms.

Photocatalytic Activity

The Co-cyt b_{562} mutants were assayed to investigate their ability to reduce CO_2 under photoinduced conditions by using $[Ru(bpy)_3]^{2+}$ as photosensitizer and ascorbic acid as sacrificial electron donor. The excited state of $[Ru(bpy)_3]^{2+}$ is reduced by ascorbic acid to $[Ru(bpy)_3]^{+}$, which in turns transfers electrons to the catalyst resulting in substrate reduction (Morris et al., 2009). The Co-cyt b_{562} mutants produced carbon monoxide and formate, in addition to H_2 produced both in the presence and absence of CO_2. Control experiments lacking CoPPIX showed little H_2 was produced and no CO or HCO_2^- were detected, indicating that these species were produced by the cobalt catalyst. The reactivity observed is in line with previous mechanistic studies of cobalt porphyrins used as catalysts for these reactions (SI, **Supplementary Figure S3**) (Dhanasekaran et al., 1999; Morris et al., 2009; Leung et al., 2010; Nielsen and Leung, 2010; Shen et al., 2016; Call et al., 2019b).

The time-dependent results of the experiments are presented in **Figure 2** and the final turnover numbers are shown on **Table 2** and **Figure 3**. When assayed under a CO_2 atmosphere at pH 6.0, all mutants showed a two-fold increase in production of CO equivalent compared to the porphyrin alone, indicating that activity is increased by the interaction of the protein with the porphyrin (**Table 2**; **Figures 2**, **3**). In contrast, activity toward formate production was similar to free porphyrin in all cases, with a slight decrease for M7A at pH 6.0. Observed H_2 production activity at pH 6.0 was in all cases higher than CoPPIX, however with significant variation between mutants: M7A showed a (20 ± 5)% increase in H_2 compared to the porphyrin alone, followed by M7H ((45 ± 7)%) and WT ((72 ± 7)%, $p = 0.64$ for the M7H and

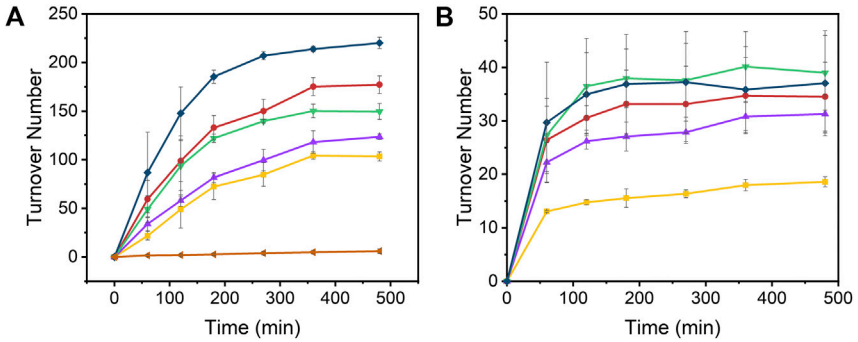

FIGURE 2 | Turnover number values of **(A)** H_2 and **(B)** CO over time from the photoinduced reduction of protons by $[Ru(bpy)_3]^{2+}$, CoPPIX, and Co-cyt b_{562} mutants at pH 6.0 under 1 atm CO_2. The experiments were carried out in 100 mM ascorbic acid, 1 mM $[Ru(bpy)_3]^{2+}$, 200 mM potassium phosphate, 20 μM CoPPIX (except in the negative control), and 30 μM of corresponding apo cyt b_{562} (except for free CoPPIX; apo WT cyt b_{562} was used for the negative control) under white LED light irradiation. Colors represent $[Ru(bpy)_3]^{2+}$ (negative control, orange side triangles), free CoPPIX (yellow squares), WT (red circles), M7A (purple up triangles), M7H (green down triangles), and H102A (dark blue diamonds). The TON for the negative control was calculated assuming a hypothetical catalyst content identical to the other samples (8 nmol) for direct comparison. The experiments were run on triplicate and error bars represent the standard deviation of the sample.

TABLE 2 | Turnover numbers for the observed products under light irradiation in 200 mM potassium phosphate, 100 mM ascorbic acid, 1 mM $[Ru(bpy)_3]^{2+}$, and 1 atm of gas.

Mutant	TON H_2			TON CO		TON HCO_2^-	
	pH 6[a]	pH 6	pH 7	pH 6	pH 7	pH 6	pH 7
CoPPIX	89 ± 6	103 ± 5	97 ± 3	19 ± 1	23 ± 1	33 ± 4	22 ± 1
WT	170 ± 12	177 ± 9	131 ± 10	35 ± 6	34 ± 6	33 ± 4	27 ± 9
M7A	126 ± 5	124 ± 3	93 ± 6	31 ± 4	36 ± 6	20 ± 3	24 ± 8
M7H	167 ± 10	150 ± 8	143 ± 6	39 ± 7	42 ± 11	38 ± 6	35 ± 14
H102A	205 ± 16	220 ± 6	163 ± 7	37 ± 10	33 ± 10	37 ± 8	25 ± 8

[a]*Control experiment under Ar instead of CO_2.*

WT comparison), and finally H102A with the highest increase in activity [(113 ± 5)%]. The assay was repeated in the absence of CO_2 (**Figure 3** and SI, **Supplementary Figure S6**), and yielded similar TON values for H_2, indicating that overall H_2 production is not affected by the presence of CO_2. Methionine coordination at position seven results in a higher overall activity, as mutants bearing this residue (WT, H102A) resulted in the highest TON values. A possible explanation of these observations is that as the metal center becomes more electron rich, a softer ligand—such as methionine's thioether side chain—is capable of better stabilizing the reduced intermediates that are formed throughout the catalytic cycle. Finally, the difference between the activities of H102A and WT could be due to the opening of a coordination site on one side of the porphyrin, thus increasing the chance of substrate binding to the active site. The near identical TONs observed for CO production as opposed to the variability observed for proton reduction suggests that the protein scaffold may provide proton relay pathways toward the active site. The rate limiting step of CO_2 reduction to CO does not involve protonation steps, thus not benefiting in the same manner from the different proton environments as the H_2-production cycle (**Supplementary Figure S3**).

The turnover numbers relative to CO production measured at pH 7.0 were generally unchanged for the holoprotein, while a

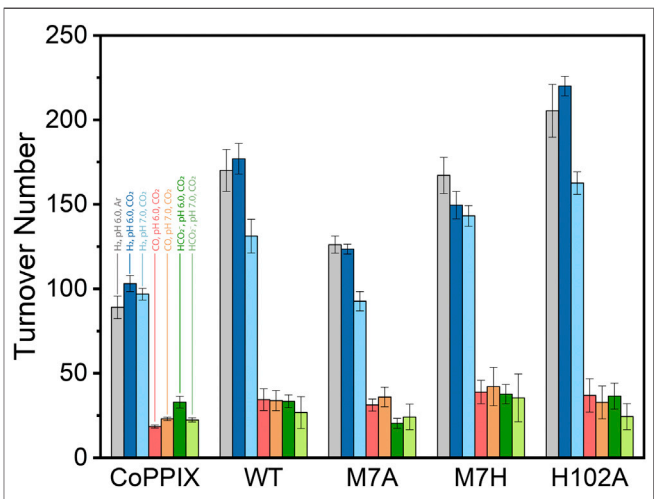

FIGURE 3 | Turnover number values obtained for CoPPIX and cobalt cyt b_{562} mutants under irradiation with light for 8 h in 100 mM ascorbic acid, 1 mM $[Ru(bpy)_3]^{2+}$, and 200 mM potassium phosphate. The bars represent the TON of each catalyst at pH 6.0 in absence (H_2: gray) and presence of CO_2 (H_2: dark blue, CO: red, HCO_2^-: dark green); and in the presence of CO_2 at pH 7 (H_2: light blue, CO: orange, HCO_2^-: light green). The experiments were run on triplicate and error bars represent the standard deviation of the sample.

slight increase was recorded for CoPPIX. Unsurprisingly the H_2 yield for WT, M7A, and H102A decreased by 20%, as proton concentration is decreased 10-fold. However, no statistically significant change was observed for the H_2 TON of the free porphyrin or the M7H mutant. Finally, a decrease in formate production was observed for the free porphyrin, consistent with the fact that its formation is dependent on proton concentration. The formate TON values for the holo proteins were not statistically different to those obtained at pH 6.0, suggesting that the protein environment might serve as a proton source throughout this particular catalytic route, thus mitigating the effect of the lower proton concentration in solution.

CONCLUSION

We have investigated the effect of the primary coordination sphere provided by the protein environment of cobalt cytochrome b_{562} in the light-promoted CO_2 reduction pathway in mild aqueous conditions. Our results indicate that the native CO_2 reduction activity of CoPPIX is increased when incorporated into the protein, whereas HCO_2^- production is not affected by the protein scaffold. Additionally, proton reduction showed a difference in activities between the mutants, suggesting that both electronic and steric effects play an important role throughout the catalytic cycle that leads to H_2 production. Three of our protein scaffolds (WT, M7A, H102A) displayed pH dependance of proton reduction activity as expected, whereas M7H and CoPPIX did not show any noticeable change in activity at the examined pH values. No pH dependence of CO_2 reduction activity was observed between the catalysts, indicating that other factors may come into play in the mechanism of CO_2 reduction by these catalysts.

This work illustrates the first example of light driven carbon dioxide reduction by a protein-cobalt porphyrin catalyst, and demonstrates that hybrid metalloenzymes can be generated by incorporating CoPPIX into cyt b_{562}; in water, the novel enzyme yields CO, formate, and hydrogen. Hydrogen production activity is modulated by mutating residues involved in the first coordination sphere of the porphyrin; in contrast, the mutations investigated here do not affect significantly CO_2 reduction. Further work explanding mutations in the first and second coordination sphere could provide insight into the mechanism(s) of photoinduced reduction of H^+ and CO_2, which in turn could result in better catalysts for renewable energy and green chemistry.

DATA AVAILABILITY STATEMENT

The original contributions presented in the study are included in the article/**Supplementary Material**, further inquiries can be directed to the corresponding author.

AUTHOR CONTRIBUTIONS

RA-T, DS, and GG conceived the idea and designed the experiments. RA-T, DS, and NG performed the experiments. RA-T, NH, and GG analyzed the data. RA-T and GG wrote the article.

FUNDING

This work was supported by NSF SusChEM under Award 1508301 to GG.

ACKNOWLEDGMENTS

The authors would like to thank Brian Cherry (ASU) for help with setting up the NMR quantification of formate, and Dr. Kirtland J. Robinson for helpful discussions. The content of this manuscript has been published in part as part of the thesis of RA-T (Alcala-Torano, 2019).

SUPPLEMENTARY MATERIAL

The Supplementary Material for this article can be found online at: https://www.frontiersin.org/articles/10.3389/fmolb.2021.609654/full#supplementary-material.

REFERENCES

Alcala-Torano, R. (2019). Rational metalloprotein design for energy conversion applications. Dissertation, Tempe (AZ): Arizona State University.

Alcala-Torano, R., Sommer, D. J., Bahrami Dizicheh, Z., and Ghirlanda, G. (2016). in *Chapter seventeen—design strategies for redox active metalloenzymes: applications in hydrogen production. Methods in Enzymology*. Editor V. L. Pecoraro (Academic Press), 389–416.

Alvarez-Hernandez, J. L., Sopchak, A. E., and Bren, K. L. (2020). Buffer pK_a impacts the mechanism of hydrogen evolution catalyzed by a cobalt porphyrin-peptide. *Inorg. Chem.* 59 (12), 8061–8069. doi:10.1021/acs.inorgchem.0c00362

Azcarate, I., Costentin, C., Robert, M., and Savéant, J.-M. (2016a). Dissection of electronic substituent effects in multielectron-multistep molecular catalysis. Electrochemical CO_2-to-CO conversion catalyzed by iron porphyrins. *J. Phys. Chem. C.* 120 (51), 28951–28960. doi:10.1021/acs.jpcc.6b09947

Azcarate, I., Costentin, C., Robert, M., and Savéant, J.-M. (2016b). Through-space charge interaction substituent effects in molecular catalysis leading to the design of the most efficient catalyst of CO_2-to-CO electrochemical conversion. *J. Am. Chem. Soc.* 138 (51), 16639–16644. doi:10.1021/jacs.6b07014

Bhugun, I., Lexa, D., and Savéant, J.-M. (1996). Catalysis of the electrochemical reduction of carbon dioxide by iron(0) porphyrins: synergystic effect of weak brönsted acids. *J. Am. Chem. Soc.* 118 (7), 1769–1776. doi:10.1021/ja9534462

Birdja, Y. Y., Vos, R. E., Wezendonk, T. A., Jiang, L., Kapteijn, F., and Koper, M. T. M. (2018). Effects of substrate and polymer encapsulation on CO_2 electroreduction by immobilized indium(III) protoporphyrin. *ACS Catal.* 8 (5), 4420–4428. doi:10.1021/acscatal.7b03386

Boston, D. J., Xu, C., Armstrong, D. W., and MacDonnell, F. M. (2013). Photochemical reduction of carbon dioxide to methanol and formate in a

homogeneous system with pyridinium catalysts. *J. Am. Chem. Soc.* 135 (44), 16252–16255. doi:10.1021/ja406074w

Bowen, B. J., McGarrity, A. R., Szeto, J.-Y. A., Pudney, C. R., and Jones, D. D. (2020). Switching protein metalloporphyrin binding specificity by design from iron to fluorogenic zinc. *Chemical Commun.* 56 (31), 4308–4311. doi:10.1039/D0CC00596G

Burke, A. J., Lovelock, S. L., Frese, A., Crawshaw, R., Ortmayer, M., Dunstan, M., et al. (2019). Design and evolution of an enzyme with a non-canonical organocatalytic mechanism. *Nature* 570 (7760), 219–223. doi:10.1038/s41586-019-1262-8

Call, A., Casadevall, C., Romero-Rivera, A., Martin-Diaconescu, V., Sommer, D. J., Osuna, S., et al. (2019a). Improved electro- and photocatalytic water reduction by confined cobalt catalysts in streptavidin. *ACS Catal.* 9 (7), 5837–5846. doi:10.1021/acscatal.8b04981

Call, A., Cibian, M., Yamamoto, K., Nakazono, T., Yamauchi, K., and Sakai, K. (2019b). Highly efficient and selective photocatalytic CO_2 reduction to CO in water by a cobalt porphyrin molecular catalyst. *ACS Catal.* 9 (6), 4867–4874. doi:10.1021/acscatal.8b04975

Chakrabartty, A., Schellman, J. A., and Baldwin, R. L. (1991). Large differences in the helix propensities of alanine and glycine. *Nature* 351 (6327), 586–588. doi:10.1038/351586a0

Chen, K., and Arnold, F. H. (2020). Engineering new catalytic activities in enzymes. *Nature Catal.* 3 (3), 203–213. doi:10.1038/s41929-019-0385-5

Costentin, C., Drouet, S., Robert, M., and Savéant, J.-M. (2012). A local proton source enhances CO_2; electroreduction to CO by a molecular Fe catalyst. *Science* 338 (6103), 90. doi:10.1126/science.1224581

Davis, H. J., and Ward, T. R. (2019). Artificial metalloenzymes: challenges and opportunities. *ACS Cent. Sci.* 5 (7), 1120–1136. doi:10.1021/acscentsci.9b00397

Dhanasekaran, T., Grodkowski, J., Neta, P., Hambright, P., and Fujita, E. (1999). *p*-Terphenyl-Sensitized photoreduction of CO_2 with cobalt and iron porphyrins. interaction between CO and reduced metalloporphyrins. *J. Phys. Chem.* 103 (38), 7742–7748. doi:10.1021/jp991423u

Drienovská, I., and Roelfes, G. (2020). Expanding the enzyme universe with genetically encoded unnatural amino acids. *Nature Catalysis.* 3 (3), 193–202. doi:10.1038/s41929-019-0410-8

Drienovská, I., Scheele, R. A., Gutiérrez de Souza, C., and Roelfes, G. (2020). A hydroxyquinoline-based unnatural amino acid for the design of novel artificial metalloenzymes. *Chembiochem.* 21, 3077–3081. doi:10.1002/cbic.202000306

Edgcomb, S. P., and Murphy, K. P. (2002). Variability in the pK_a of histidine side-chains correlates with burial within proteins. *Proteins: Structure, Function, and Bioinformatics.* 49 (1), 1–6. 10.1002/prot.10177

Edwards, E. H., and Bren, K. L. (2020). Light-driven catalysis with engineered enzymes and biomimetic systems. *Biotechnol. Appl. Biochem.* 67, 463–483. doi:10.1002/bab1976

Feng, L., Wang, K.-Y., Joseph, E., and Zhou, H.-C. (2020). Catalytic porphyrin framework compounds. *Trends Chem.* 2 (6), 555–568. doi:10.1016/j.trechm.2020.01.003

Feng, Y., Sligar, S. G., and Wand, A. J. (1994). Solution structure of apocytochrome b_{562}. *Nat. Struct. Biol.* 1 (1), 30–35. doi:10.1038/nsb0194-30

Firpo, V., Le, J. M., Pavone, V., Lombardi, A., and Bren, K. L. (2018). Hydrogen evolution from water catalyzed by cobalt-monochrome VI*a, a synthetic mini-protein. *Chem. Sci.* 9 (45), 8582–8589. doi:10.1039/C8SC01948G

Fukuzumi, S., Lee, Y.-M., and Nam, W. (2019). Photocatalytic redox reactions with metalloporphyrins. *J. Porphyr. Phthalocyanines* 24 (01n03), 21–32. doi:10.1142/S1088424619300131

Hay, S., and Wydrzynski, T. (2005). Conversion of the *Escherichia coli* cytochrome b_{562} to an archetype cytochrome *b*: A mutant with bis-histidine ligation of heme iron. *Biochemistry* 44 (1), 431–439. doi:10.1021/bi0492298

Hulme, E. C., and Trevethick, M. A. (2010). Ligand binding assays at equilibrium: validation and interpretation. *Br. J. Pharmacol.* 161 (6), 1219–1237. doi:10.1111/j.1476-5381.2009.00604.x

Jeong, W. J., Yu, J., and Song, W. J. (2020). Proteins as diverse, efficient, and evolvable scaffolds for artificial metalloenzymes. *Chemical Commun.* 56 (67), 9586–9599. doi:10.1039/D0CC03137B

Kamiya, N., Okimoto, Y., Ding, Z., Ohtomo, H., Shimizu, M., Kitayama, A., et al. (2001). How does heme axial ligand deletion affect the structure and the function of cytochrome b_{562}? *Protein Eng. Des. Sel.* 14 (6), 415–419. doi:10.1093/protein/14.6.415

Kleingardner, J. G., Kandemir, B., and Bren, K. L. (2014). Hydrogen evolution from neutral water under aerobic conditions catalyzed by cobalt microperoxidase-11. *J. Am. Chem. Soc.* 136 (1), 4–7. doi:10.1021/ja406818h

Kondo, M., Ichii, K., Patra, P. K., Poulter, B., Calle, L., Koven, C., et al. (2018). Plant regrowth as a driver of recent enhancement of terrestrial CO_2 uptake. *Geophys. Res. Lett.* 45 (10), 4820–4830. doi:10.1029/2018GL077633

Kornienko, N., Zhao, Y., Kley, C. S., Zhu, C., Kim, D., Lin, S., et al. (2015). Metal-organic frameworks for electrocatalytic reduction of carbon dioxide. *J. Am. Chem. Soc.* 137 (44), 14129–14135. doi:10.1021/jacs.5b08212

Kovacs, E., Tóth, J., Vértessy, B. G., and Liliom, K. (2010). Dissociation of calmodulin-target peptide complexes by the lipid mediator sphingosylphosphorylcholine: implications in calcium signaling. *J. Biol. Chem.* 285 (3), 1799–1808. doi:10.1074/jbc.M109.053116

Kramer, W. W., and McCrory, C. C. L. (2016). Polymer coordination promotes selective CO_2 reduction by cobalt phthalocyanine. *Chem. Sci.* 7 (4), 2506–2515. doi:10.1039/C5SC04015A

Lacis, A. A., Schmidt, G. A., Rind, D., and Ruedy, R. A. (2010). Atmospheric CO_2: principal control knob governing earth's temperature. *Science* 330 (6002), 356. doi:10.1126/science.1190653

Laureanti, J. A., Ginovska, B., Buchko, G. W., Schenter, G. K., Hebert, M., Zadvornyy, O. A., et al. (2020). A positive charge in the outer coordination sphere of an artificial enzyme increases CO_2 hydrogenation. *Organometallics* 39 (9), 1532–1544. doi:10.1021/acs.organomet.9b00843

Le, J. M., Alachouzos, G., Chino, M., Frontier, A. J., Lombardi, A., and Bren, K. L. (2020). Tuning mechanism through buffer dependence of hydrogen evolution catalyzed by a cobalt mini-enzyme. *Biochemistry* 59 (12), 1289–1297. doi:10.1021/acs.biochem.0c00060

Le, J. M., and Bren, K. L. (2019). Engineered enzymes and bioinspired catalysts for energy conversion. *ACS Energy Letters.* 4 (9), 2168–2180. doi:10.1021/acsenergylett.9b01308

Lee, C. H., Dogutan, D. K., and Nocera, D. G. (2011). Hydrogen generation by hangman metalloporphyrins. *J. Am. Chem. Soc.* 133 (23), 8775–8777. doi:10.1021/ja202136y

Leung, K., Nielsen, I. M. B., Sai, N., Medforth, C., and Shelnutt, J. A. (2010). Cobalt-porphyrin catalyzed electrochemical reduction of carbon dioxide in water. 2. mechanism from first principles. *J. Phys. Chem.* 114 (37), 10174–10184. doi:10.1021/jp1012335

Liang, A. D., Serrano-Plana, J., Peterson, R. L., and Ward, T. R. (2019). Artificial metalloenzymes based on the biotin–streptavidin technology: enzymatic cascades and directed evolution. *Acc. Chem. Res.* 52 (3), 585–595. doi:10.1021/acs.accounts.8b00618

Lin, S., Diercks, C. S., Zhang, Y.-B., Kornienko, N., Nichols, E. M., Zhao, Y., et al. (2015). Covalent organic frameworks comprising cobalt porphyrins for catalytic CO_2 reduction in water. *Science* 349 (6253), 1208. doi:10.1126/science.aac8343

Liu, X., Kang, F., Hu, C., Wang, L., Xu, Z., Zheng, D., et al. (2018). A genetically encoded photosensitizer protein facilitates the rational design of a miniature photocatalytic CO_2-reducing enzyme. *Nat. Chem.* 10 (12), 1201–1206. doi:10.1038/s41557-018-0150-4

Liu, Y., and McCrory, C. C. L. (2019). Modulating the mechanism of electrocatalytic CO_2 reduction by cobalt phthalocyanine through polymer coordination and encapsulation. *Nat. Commun.* 10 (1), 1683. doi:10.1038/s41467-019-09626-8

Lu, Y., Yeung, N., Sieracki, N., and Marshall, N. M. (2009). Design of functional metalloproteins. *Nature* 460, 855. doi:10.1038/nature08304

Luan, G., and Lu, X. (2018). Tailoring cyanobacterial cell factory for improved industrial properties. *Biotechnol. Adv.* 36 (2), 430–442. doi:10.1016/j.biotechadv.2018.01.005

Ma, B., Chen, G., Fave, C., Chen, L., Kuriki, R., Maeda, K., et al. (2020). Efficient visible-light-driven CO_2 reduction by a cobalt molecular catalyst covalently linked to mesoporous carbon nitride. *J. Am. Chem. Soc.* 142 (13), 6188–6195. doi:10.1021/jacs.9b13930

Manbeck, G. F., and Fujita, E. (2015). A review of iron and cobalt porphyrins, phthalocyanines and related complexes for electrochemical and photochemical reduction of carbon dioxide. *J. Porphyr. Phthalocyanines* 19 (01-03), 45–64. doi:10.1142/S1088424615300013

Markel, U., Essani, K. D., Besirlioglu, V., Schiffels, J., Streit, W. R., and Schwaneberg, U. (2020). Advances in ultrahigh-throughput screening for

directed enzyme evolution. *Chem. Soc. Rev.* 49 (1), 233–262. doi:10.1039/C8CS00981C

Mondal, B., Rana, A., Sen, P., and Dey, A. (2015). Intermediates involved in the $2e^-/2H^+$ reduction of CO_2 to CO by iron(0) porphyrin. *J. Am. Chem. Soc.* 137 (35), 11214–11217. doi:10.1021/jacs.5b05992

Morris, A. J., Meyer, G. J., and Fujita, E. (2009). Molecular approaches to the photocatalytic reduction of carbon dioxide for solar fuels. *Acc. Chem. Res.* 42 (12), 1983–1994. doi:10.1021/ar9001679

Nastri, F., D'Alonzo, D., Leone, L., Zambrano, G., Pavone, V., and Lombardi, A. (2019). Engineering metalloprotein functions in designed and native scaffolds. *Trends Biochem. Sci.* 44 (12), 1022–1040. doi:10.1016/j.tibs.2019.06.006

Nielsen, I. M. B., and Leung, K. (2010). Cobalt-porphyrin catalyzed electrochemical reduction of carbon dioxide in water. 1. A density functional study of intermediates. *J. Phys. Chem.* 114 (37), 10166–10173. doi:10.1021/jp101180m

Onoda, A., Kihara, Y., Fukumoto, K., Sano, Y., and Hayashi, T. (2014). Photoinduced hydrogen evolution catalyzed by a synthetic diiron dithiolate complex embedded within a protein matrix. *ACS Catal.* 4 (8), 2645–2648. doi:10.1021/cs500392e

Oohora, K., Onoda, A., and Hayashi, T. (2019). Hemoproteins reconstituted with artificial metal complexes as biohybrid catalysts. *Acc. Chem. Res.* 52 (4), 945–954. doi:10.1021/acs.accounts.8b00676

Pace, C. N., and Scholtz, J. M. (1998). A helix propensity scale based on experimental studies of peptides and proteins. *Biophys. J.* 75 (1), 422–427. 10.1016/S0006-3495(98)77529-0

Pia, E. A. D., Chi, Q., Elliott, M., Emyr Macdonald, J., Ulstrup, J., and Dafydd Jones, D. (2012). Redox tuning of cytochrome b_{562} through facile metal porphyrin substitution. *Chemical Communications* 48 (86), 10624–10626. doi:10.1039/C2CC34302A

Rao, H., Lim, C.-H., Bonin, J., Miyake, G. M., and Robert, M. (2018). Visible-light-driven conversion of CO_2 to CH_4 with an organic sensitizer and an iron porphyrin catalyst. *J. Am. Chem. Soc.* 140 (51), 17830–17834. doi:10.1021/jacs.8b09740

Roy, A., Madden, C., and Ghirlanda, G. (2012). Photo-induced hydrogen production in a helical peptide incorporating a [FeFe] hydrogenase active site mimic. *Chemical Commun.* 48 (79), 9816–9818. doi:10.1039/C2CC34470J

Roy, A., Vaughn, M. D., Tomlin, J., Booher, G. J., Kodis, G., Simmons, C. R., et al. (2020). Enhanced photocatalytic hydrogen production by hybrid streptavidin-diiron catalysts. *Chemistry* 26 (28), 6240–6246. doi:10.1002/chem.202000204

Sano, Y., Onoda, A., and Hayashi, T. (2011). A hydrogenase model system based on the sequence of cytochrome c: photochemical hydrogen evolution in aqueous media. *Chemical Commun.* 47 (29), 8229–8231. doi:10.1039/C1CC11157D

Schneider, C. R., Manesis, A. C., Stevenson, M. J., and Shafaat, H. S. (2018). A photoactive semisynthetic metalloenzyme exhibits complete selectivity for CO_2 reduction in water. *Chemical Commun.* 54 (37), 4681–4684. doi:10.1039/C8CC01297K

Schneider, C. R., and Shafaat, H. S. (2016). An internal electron reservoir enhances catalytic CO_2 reduction by a semisynthetic enzyme. *Chemical Commun.* 52 (64), 9889–9892. doi:10.1039/C6CC03901D

Schwizer, F., Okamoto, Y., Heinisch, T., Gu, Y., Pellizzoni, M. M., Lebrun, V., et al. (2018). Artificial metalloenzymes: reaction scope and optimization strategies. *Chem. Rev.* 118 (1), 142–231. doi:10.1021/acs.chemrev.7b00014

Shen, J., Kolb, M. J., Göttle, A. J., and Koper, M. T. M. (2016). DFT study on the mechanism of the electrochemical reduction of CO_2 catalyzed by cobalt porphyrins. *J. Phys. Chem. C* 120 (29), 15714–15721. doi:10.1021/acs.jpcc.5b10763

Slater, J. W., Marguet, S. C., Gray, M. E., Monaco, H. A., Sotomayor, M., and Shafaat, H. S. (2019). Power of the secondary sphere: modulating hydrogenase activity in nickel-substituted rubredoxin. *ACS Catal.* 8928–8942. doi:10.1021/acscatal.9b01720

Smith, P., Davis, S. J., Creutzig, F., Fuss, S., Minx, J., Gabrielle, B., et al. (2015). Biophysical and economic limits to negative CO_2 emissions. *Nat. Clim. Change* 6, 42. doi:10.1038/nclimate2870

Sommer, D. J., Vaughn, M. D., Clark, B. C., Tomlin, J., Roy, A., and Ghirlanda, G. (2016). Reengineering cyt b_{562} for hydrogen production: a facile route to artificial hydrogenases. *Biochim. Biophys. Acta Bioenerg.* 1857 (5), 598–603. doi:10.1016/j.bbabio.2015.09.001

Sommer, D. J., Vaughn, M. D., and Ghirlanda, G. (2014). Protein secondary-shell interactions enhance the photoinduced hydrogen production of cobalt protoporphyrin IX. *Chemical Commun.* 50 (100), 15852–15855. doi:10.1039/C4CC06700B

Sun, Y., Gu, L., Dickinson, R. E., Norby, R. J., Pallardy, S. G., and Hoffman, F. M. (2014). Impact of mesophyll diffusion on estimated global land CO_2 fertilization. *Proc. Natl. Acad. Sci. Unit. States Am.* 111, 15774–15779. doi:10.1073/pnas.1418075111

Thordarson, P. (2011). Determining association constants from titration experiments in supramolecular chemistry. *Chem. Soc. Rev.* 40 (3), 1305–1323. doi:10.1039/C0CS00062K

Vornholt, T., Christoffel, F., Pellizzoni, M. M., Panke, S., Ward, T. R., and Jeschek, M. (2020). Systematic engineering of artificial metalloenzymes for new-to-nature reactions, *bioRxiv*. 2007, 204206. doi:10.1101/2020.07.15.204206

Walsh, A. P., Laureanti, J. A., Katipamula, S., Chambers, Geoffrey. M., Priyadarshani, N., Lense, S., et al. (2019). Evaluating the impacts of amino acids in the second and outer coordination spheres of Rh-bis(diphosphine) complexes for CO_2 hydrogenation. *Faraday Discuss* 215 (0), 123–140. doi:10.1039/C8FD00164B

Woo, H. M. (2017). Solar-to-chemical and solar-to-fuel production from CO_2 by metabolically engineered microorganisms. *Curr. Opin. Biotechnol.* 45, 1–7. doi:10.1016/j.copbio.2016.11.017

Wu, Q., Xie, R.-K., Mao, M.-J., Chai, G.-L., Yi, J.-D., Zhao, S.-S., et al. (2020). Integration of strong electron transporter tetrathiafulvalene into metalloporphyrin-based covalent organic framework for highly efficient electroreduction of CO_2. *ACS Energy Letters* 5 (3), 1005–1012. doi:10.1021/acsenergylett.9b02756

Yehezkeli, O., Bedford, N. M., Park, E., Ma, K., and Cha, J. N. (2016). Semiconductor-based, solar-driven photochemical cells for fuel generation from carbon dioxide in aqueous solutions. *ChemSusChem.* 9 (22), 3188–3195. doi:10.1002/cssc.201601105

Zhang, H., Wei, J., Dong, J., Liu, G., Shi, L., An, P., et al. (2016). Efficient visible-light-driven carbon dioxide reduction by a single-atom implanted metal-organic framework. *Angew. Chem. Int. Ed.* 55 (46), 14310–14314. doi:10.1002/anie.201608597

Zhang, X.-D., Hou, S.-Z., Wu, J.-X., and Gu, Z.-Y. (2020). Two-dimensional metal–organic framework nanosheets with cobalt-porphyrins for high-performance CO_2 electroreduction. *Chem. Eur J.* 26 (7), 1604–1611. doi:10.1002/chem.201904072

Zhang, X., Wu, Z., Zhang, X., Li, L., Li, Y., Xu, H., et al. (2017). Highly selective and active CO_2 reduction electrocatalysts based on cobalt phthalocyanine/carbon nanotube hybrid structures. *Nat. Commun.* 8, 14675. doi:10.1038/ncomms14675

Zhou, Z., and Roelfes, G. (2020). Synergistic catalysis in an artificial enzyme by simultaneous action of two abiological catalytic sites. *Nature Catalysis.* 3 (3), 289–294. doi:10.1038/s41929-019-0420-6

Conflict of Interest: The authors declare that the research was conducted in the absence of any commercial or financial relationships that could be construed as a potential conflict of interest.